Regular Article

ANALYTICAL
AND BIOANALYTICAL
CHEMISTRY
RESEARCH

Published by the
Iranian Chemical Society

***Anal. Bioanal. Chem. Res.**, Vol. 10, No. 3, 363-373, July 2023.*

A Copper-Based Metal-Organic Framework/Molecularly Imprinted Polymer-Modified Graphite Epoxy Composite Electrode for the Electrochemical Detection of Chlorpyrifos and Investigating Optimum Conditions with the aid of Quantum-Mechanical DFT Calculations

Fariba Beigmoradi, Masoud Rohani Moghadam*, Alireza Bazmandegan-Shamili and Hamid Reza Masoodi

Department of Chemistry, Faculty of Sciences, Vali-e-Asr University of Rafsanjan, Rafsanjan, Iran

(Received 20 February 2023, Accepted 8 April 2023)

In this study, a new electrochemical sensor using MIPs coated on the surface of Cu-MOF was developed for the selective determination of chlorpyrifos (CPF). Cu-MOF (HKUST-1) was synthesized based on a solvothermal method. Molecularly imprinted polymers (MIPs) were prepared using chlorpyrifos as the template molecule, methacrylic acid as the functional monomer, and ethylene glycol dimethyacrylate as the cross-linker. The optimum pH value of the rebinding solution was verified with computational calculations obtained by Gaussian software. The HKUST-1@MIP was characterized by several techniques, including Fourier-transform infrared spectroscopy (FT-IR), field-emission scanning electron microscopy (FESEM), and X-ray diffraction (XRD). HKUST-1@MIP/GEC electrode showed an excellent linear range of 0.01 to 1.00 µM, with RSD% and LOD of 5.37% and 3 nM, respectively. The modified electrode presents a simple, selective, sensitive, stable, and environmentally friendly strategy for the determination of CPF. The proposed method was successfully used to measure CPF in apple and tomato samples.

Keywords: Electrochemical sensor, HKUST-1@MIPs, Quantum mechanic-DFT, Chlorpyrifos

INTRODUCTION

O,O-Diethyl-O-3,5,6-trichloropyridin-2-yl phosphorothioate or chlorpyrifos (CPF) is an organophosphate pesticide used broadly in rural and urban farming to control insects [1]. In the insect's body, CPF inhibits the acetylcholinesterase enzyme. Acetylcholine acts as a neurotransmitter in the inter-synaptic space. Accumulating acetylcholine causes continuous nervous system stimulation, eventually killing the insect [2]. Humans can be exposed to CPF through ingestion, inhalation, or absorption from the skin. This pesticide has harmful human effects, including neurological ailments, muscular dystrophy, respiratory disorder, and sometimes death [3]. Therefore, it is crucial to determine the CPF residual in environmental samples and agricultural products.

Several analytical techniques, such as High-Performance Liquid Chromatography (HPLC- UV-Vis spectrophotometry) [4,5], Gas Chromatography (GC- ion mobility spectrometry (IMS) and mass spectrometry (MS)) [6,7], colorimetry- UV-Vis spectrophotometry [8], solid-phase microextraction (SPME- UV-Vis spectrophotometry) [9], and electrochemistry [10] have been developed for this purpose. Although these techniques are selective and sensitive, some are time-consuming, have expensive instrumentation, and need intricate sample pretreatment [11]. On the other hand, electrochemical techniques are fast, sensitive, and low-cost in procedure and instrument [12,13].

Molecularly imprinted polymers (MIPs) are usually synthesized by polymerizing the functional monomer and

*Corresponding author. E-mail: m.rohani@vru.ac.ir

crosslinking agent in the presence of target molecules. After removing the template molecule from the polymer matrix, numerous 3D cavities remain matched with the analyte in size, shape, and functional groups [14]. MIPs promise stable, selective materials under harsh chemical and physical conditions [15]. Nowadays, several methods, such as precipitation polymerization [16], sol-gels [17], solid-phase synthesis [18], electropolymerization [19], emulsion polymerization [20], and bulk polymerization [21] have been developed for the synthesis of MIPs.

Metal-organic frameworks (MOFs), denominated as porous coordination polymers (PCPs), have emerged as a relatively new category of nanoporous materials [22]. They are formed by the self-assembling of metal ions/metal clusters and organic ligands by coordination. The benefits of MOFs are a large surface area, ultra-high porosity, non-toxic nature, chemical functionality, and stable framework. MOFs have been generally used in different fields, such as gas storage [23], separation [24], catalysis [25], nonlinear optics [26], drug delivery [27], and also sensors [28]. Cu-based MOF, also known as HKUST-1, is a notable MOF with various applications. Its electrochemical utilization is due to superior electrocatalytic specifications and the changeable valency of Cu [29].

Epoxy resins are compounds with more than one epoxy group that are cured with a broad range of co-reactants, including acid anhydrides, polyamides, polyfunctional amines, phenols, alcohols, and thiols for the formation of thermosetting polymers. These agents react with epoxy resin during the curing process to form cross-links and a three-dimensional network [30]. Epoxy resins have properties such as high mechanical, chemical, and temperature resistance. Epoxy resins, as inexpensive, robust, and conductive materials (*e.g.* graphite), are widely used in electrochemical sensors [31].

In this study, a sensitive and highly selective electrochemical sensor was fabricated using a graphite-epoxy composite electrode (GECE) based on HKUST-1@MIPs. According to the characteristics mentioned for MOF, especially porosity and high surface area, it has been used in various fields, especially in electrochemical sensors and in this work. But their problem is low conductivity in pure form, and to solve this problem, they must be composited with conductive compounds [32]. For this reason, in this work, MOF, which has a large surface area, is used as a substrate for the formation of MIPs on it, and in this way, the conductivity of MOF increases. Thus, initially, HKUST-1 was synthesized based on a solvothermal method. Then, MIPs were synthesized on the HKUST-1 surface using ethylene glycol dimethyl acrylate (EGDMA) as a cross-linker, methacrylic acid (MAA) as a functional monomer, and 2,2'-azobisisobutyronitrile (AIBN) as an initiator in the presence of the CPF molecule. HKUST-1@MIPs were prepared after removing CPF from MIPs. Then graphite, epoxy resin, and HKUST-1@MIP were thoroughly mixed and filled in a homemade electrode. Also, the environmental pH can affect the geometry, energy, and properties of most systems. So here, the effect of solution pH on analyte extraction into the MIP layer is complex and ambiguous. Therefore, to clarify this effect, the stability of the CPF-MAA complex in alkaline, neutral and acidic environments has been investigated with the help of quantum mechanical calculations (DFT).

EXPERIMENTAL

Materials

MAA, EGDMA, AIBN, Chlorpyrifos (CPF), fenthion (FT), methyl parathion (MP), phosalone (PLN), and phoxim (PX) were prepared from Sigma-Aldrich (Steinheim, Germany, www.sigmaaldrich.com). Benzene-1,3,5-tricarboxylic acid (H_3BTC), copper nitrate trihydrate ($Cu(NO_3)_2.3H_2O$), chloroform, NaOH, ethanol, and H_3PO_4 were prepared from Merck (Darmstadt, Germany, www.merckgroup.com). Spectroscopic-grade graphite powder was purchased from Ringsdorff-Werke GMBH (Germany). Epoxy resin was prepared from a commercial Araldite@epoxy resin from Ciba-Geigy, Switzerland. All solutions were prepared using ultrapure water gained from a water purifier Milli-Q Gradient System A10, Millipore (USA). A standard stock solution of CPF was prepared in ethanol at 0.01 M. Freshly working solutions were prepared by diluting the necessary stock with purified water. Several phosphate buffer solutions in the pH range of 4.0-10.0 comprised 0.1 M H_3PO_4 and 0.1 M NaOH. Before performing the test, it was purged with nitrogen gas for five minutes. Fruits samples were purchased from regional supermarkets in Rafsanjan, Iran's Kerman province.

Instrumentation

All electrochemical measurements were performed using Autolab Meterohm PGSTAT204 (Switzerland, www.metrohm.com) in a three-electrode system including an Ag/AgCl as reference electrode, a platinum wire as the auxiliary electrode, and the graphite-epoxy composite modified electrode with an internal diameter of 2 mm as the working electrode. The pH measurements were carried out using a Metrohm 827 pH meter (Switzerland, www.metrohm.com) with a combined glass-calomel electrode. The morphology and Energy-dispersive X-ray spectroscopy (ED) of the synthesized MIP and HKUST-1@MIP were investigated using field emission scanning electron microscope (FE-SEM) Zeiss Sigma-VP FESEM instrument (Jena, Germany, http://www.zeiss.com). The X-ray diffraction pattern (XRD) of the synthesized MIP and HKUST-1@MIP was investigated using X' Pert Pro instrument (PANalytical Holland, https://www.malvernpanalytical.com). The FT-IR spectra were investigated using a Nicolet iS10 FT-IR spectrophotometer (Thermo Fisher Scientific, USA, https://www.thermofisher.com).

Methods

Computational analysis. Geometries and energies have been determined using the Gaussian 09 suite of programs. Since most of the actual chemistry takes place in a solvent, the calculations have been implemented in water. Considering solvents as separate molecules significantly increases the computational cost of modelling a solvent-mediated chemical reaction. So, the polarizable continuum model (PCM) has been introduced by Tomasi and coworkers [33]. In the PCM model, the structureless polarizable medium of the bulk of solvent is mainly defined based on its dielectric constant [34]. Here, the influence of water solvent on the stability of the CPF-MAA complex is theoretically examined using the PCM model at the M06-2X/6-311++G(d,p) level.

Synthesis of HKUST-1

According to the literature report [35], a solvothermal method was used to synthesize HKUST-1. For this purpose, 1.087 g of $Cu(NO_3)_2.3H_2O$ and 0.525 g of H_3BTC were dissolved in 15 ml of deionized water and 15 ml of ethanol, respectively. Then the solutions were mixed and stirred for 30 min at room temperature. Afterward, it was transferred to a 50 ml Teflon autoclave and heated at 120 °C for 12 h. The obtained blue powder was recovered and washed five times with water: ethanol (1:2) and dried for 24 h at 150 °C under an air atmosphere.

Synthesis of HKUST-1@MIPs

The synthesis of HKUST-1@MIPs was achieved according to a method reported by Asfaram *et al*., with minor adjustments [36]. For this purpose, 0.05 g of HKUST-1 and 8 ml of chloroform were added into a 100 ml round-bottomed flask and sonicated for 20 min. Then, 300 µl of MAA and 0.02 g of CPF were transported to the flask and stirred for one hour to form a monomer-template molecule complex. Afterward, 5.0 ml of EGDMA and 0.05 g of AIBN were added, and N_2 gas was passed through the solution about 10 min before 15 min of stirring. The flask was tightly closed and placed in an oil bath at 60 °C for 12 h with magnetic stirring. After polymerization, the flask was opened, and excess solvent was evaporated at room temperature. The formed polymer was dried overnight at room temperature. In order to extract the template molecule from the MIP network, a Soxhlet system with methanol: chloroform mixture (9:1 v/v) was used for 48 h and dried in an oven at 40 °C for one hour. Non-imprinted polymers (NIPs) were also prepared according to the method mentioned earlier, except for CPF addition. Also, the MIP was synthesized according to the HKUST-1@MIP synthesis without the HKUST-1.

Construction of the Graphite-Epoxy Composite Electrode

In order to make the bare graphite-epoxy composite (BGEC) electrode, the epoxy resin, and the hardener were mixed in an equal weight ratio. Then, graphite powder was added with a 10:1 (w/w) ratio and mixed by hand for 30 min to get a homogeneous mixture. Next, the prepared paste was compacted into a 2 mm diameter Teflon tube. For the electrical connection, the tube was fixed with a copper wire. HKUST-1@MIPs modified graphite-epoxy composite (HKUST-1@MIPs-MGEC) electrode was prepared in the same manner, but the graphite powder was first mixed thoroughly by hand with HKUST-1@MIPs with 9:1 (W/W) ratio. The MIPs-modified graphite-epoxy composite (MIPs-

MGEC) electrode was made using MIPs without HKUST-1. Before every test, the cross-section of the electrodes was polished with emery paper (#2500). The final polishing was done with a 0.3 μm alumina suppression to obtain electrodes with a smooth and uniform surface (Fig. S1). Then the electrode was washed thoroughly with ultra-pure water.

Real Sample Preparation

In order to evaluate the ability of the proposed sensor to measure CPF, the ready sensor was used to determine CPF in apple and tomato samples. The edible part of the samples was washed with ultrapure water and dried at room temperature for 24 h. Then they were juiced with a juicer, and 20 ml juice was centrifuged for 20 min at 4000 rpm. The liquid phase was stored at 4 °C for CPF analysis. Furthermore, specific amounts of CPF were added to the liquid phase for the spiked recovery experiments.

Measurement Procedure

After adjustment of the pH of the CPF solution to 7.0 using phosphate buffer, the HKUST-1@MIPs-GEC electrode was immersed for 8 min into the solution to bind CPF with imprint sites. Then, the loaded electrode was washed with ultrapure water to remove unbound CPF molecules and excess reagents. Afterward, the electrode dipped into a 0.1 M phosphate buffer (pH 7.0) in the electrochemical cell for analysis with differential pulse voltammetry (DPV).

RESULTS AND DISCUSSION

FESEM Characterization

The HKUST-1 and HKUST-1@MIPs morphological structures were investigated by Field emission scanning electron microscope (FESEM). Figure S2A shows a FESEM image of the synthesized HKUST-1. The noticeable crystals are octahedral with approximately the same size distribution. Figure also reveals that an enormous surface area is attained with the synthesized HKUST-1. Figure S2B shows a FESEM image of the synthesized HKUST-1@MIPs. Significant pores are observed on the smooth surface of the polymeric structure.

FT-IR Analysis

Figure 1 displays the FT-IR spectra of HKUST-1, MIPs, and HKUST-1@MIPs. For HKUST-1, the broadband peak in the range of 2900-3600 cm^{-1} corresponds to stretching the O-H bond of BTC molecules in the MOF structure. The peak at 1701 cm^{-1} corresponds to the C=O stretching mode in the carboxylic acid groups of BTC. The peaks at 1371 cm^{-1} and 725 cm^{-1} correspond to the C=C aromatic ring stretching vibration and C–H bending mode of BTC molecules, respectively. For MIPs, the peaks in 1722 and 2955 cm^{-1} correspond to C=O and C–H bending vibrations of MAA in the MIPs structure. The FT-IR spectra of MIPs and HKUST-1@MIPs are the same, implying that the surface of HKUST-1 is wholly covered with MIPs.

XRD Analysis

Figure 2 shows the X-ray diffraction pattern (Cu K_α radiation source, λ = 0.154056 nm) of the HKUST-1 and HKUST-1@MIPs. XRD of HKUST-1 implies the formation of face-centered cubic (fcc) crystallines that agree with other reports [37]. Since the MIP layer coated on the surface of HKUST-1 has an amorphous structure, no significant major peaks are observed in the HKUST-1@MIPs XRD pattern. However, the weak signals of HKUST-1, including 2Θ of 13.55, 16.60, and 17.57, can be identified in the HKUST-1@MIPs pattern.

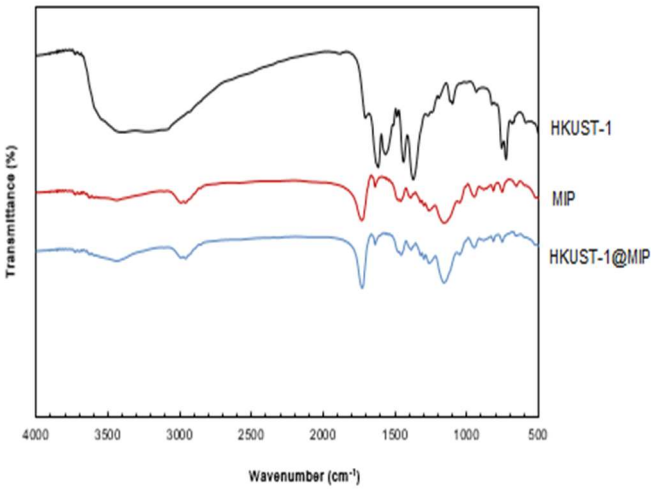

Fig. 1. FT-IR spectra of HKUST-1, MIPs, HKUST-1@MIPs.

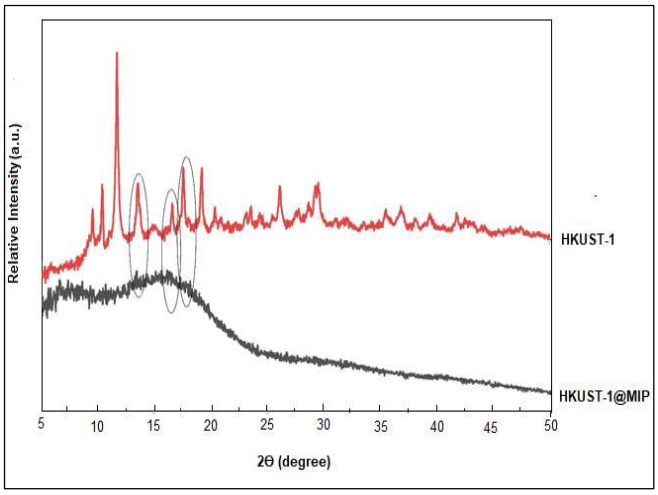

Fig. 2. XRD pattern of HKUST-1 and HKUST-1@MIP combinations.

EDX Analysis

Figures S3A and B show the EDX analysis of HKUST-1 and HKUST-1@MIPs. As shown, the amount of copper in HKUST-1 (Fig. S3A) is reduced when its surface is coated with the polymeric layer in HKUST-1@MIP (Fig. S3B). Instead, the percentage of carbon in Fig. S3B is more than in Fig. S3A due to the presence of MIP in the structure. Furthermore, P, S, and Cl are derived only from the CPF molecule (Fig. S3B). These confirm that HKUST-1@MIP synthesis has been done successfully.

Electrochemical Properties of the Electrodes

The cyclic voltammetry (CV) technique was used to study the electrochemical properties of the prepared electrodes. For this purpose, a probe solution of 6 mM $[Fe(CN)_6]^{3-/4-}$ in 0.1 M KCl was used in the potential range of -0.2 V to 0.7 V with a scan rate of 100 mV s^{-1}. A reversible CV peak pair at about 0.2 V is obtained (Fig. 3A, curve a) for the bare electrode. The electrical current obtained with MIP-GECE is more prominent (Fig. 3A, curve d) compared to NIP-GECE (Fig. 3A, curve b) due to the higher porosity and conductivity of the polymeric layer. The current increases with the HKUST-1@MIP electrode (Fig. 3A, curve e), with a more significant surface area available with HKUST-1.

Electrochemical Impedance Spectroscopy (EIS) of the probe solution was also employed to study the electrical properties of the electrodes. As shown in Fig. 3B, the bare GECE (curve a) and NIP-GECE (curve b) show big semicircular due to their higher electron-transfer resistance than the others. The electron-transfer resistance value was reduced when MIP was added to the electrode. So a tiny semicircular was observed (curve d). In curve d, the smallest semicircular is observed when the MIP is coated on the HKUST-1.

Figure 4 shows the reduction equation of CPF, which is related to the reduction of -C=N of the pyridine ring of CPF [38]. Furthermore, the electrochemical behavior of the electrodes in the presence of CPF was studied. For this purpose, different electrodes were dipped in CPF solutions,

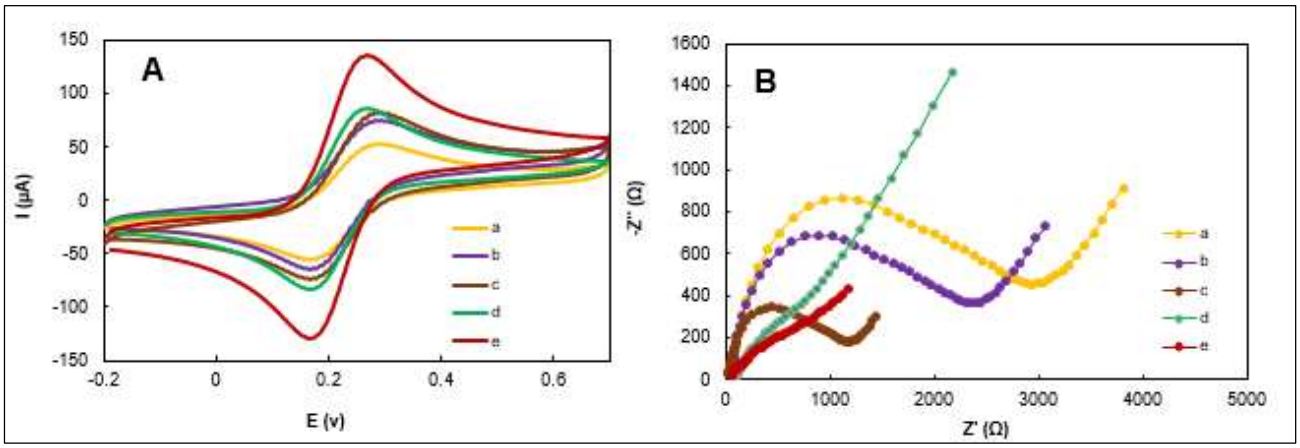

Fig. 3. A, Cyclic voltammograms of Bare GECE (a), NIP-GECE (b), HKUST-1-GECE (c), MIP-GECE (d), HKUST-1@MIP-GECE (e), and B, EIS diagrams of bare GECE (a), NIP-GECE (b), HKUST-1-GECE (c), MIP-GECE (d), and HKUST-1@MIP-GECE (e), in 6 mM $[Fe(CN)_6]^{3-/4-}$ and 0.1 M KCl with a scan rate of CV was 100 mV s^{-1} also the frequency range of EIS was from 0.0001 to 10 kHz, with amplitude of 0.2 V.

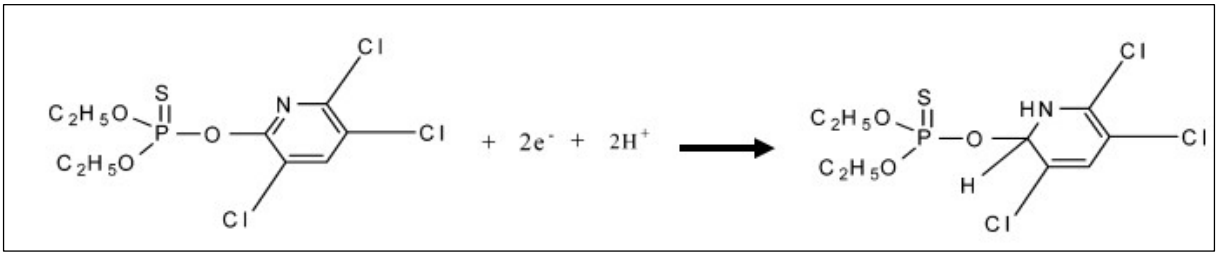

Fig. 4. Mechanism of reduction of CPF.

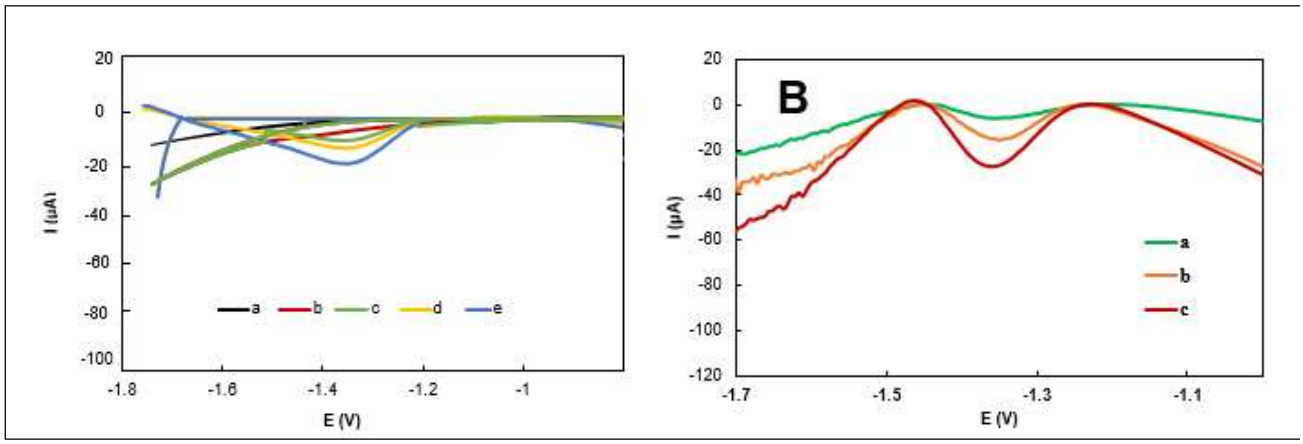

Fig. 5. A: CVs of Bare GECE in blank (a), and bare GECE (b), Cu-MOF-GECE (c), MIP-GECE (d), Cu-MOF@MIP-GECE (e) after extraction in 3.0 µM CPF in 0.1 M phosphate buffer (pH 7.0) containing 1 M KCl in the potential range of -1.0 to -1.75 V (*vs*. Ag/AgCl) and the scan rate of 50 mV s^{-1} (b), and B: DPVs of CPF for Bare GECE (a), MIP-GECE (b), and Cu-MOF@MIP-GECE (c) in 0.1 M phosphate buffer (pH 7.0) with 25.0 µM CPF in the potential range of -1.0 to -1.7 V (*vs*. Ag/AgCl) (The accumulation time of CPF is 8 min).

and their behavior was studied directly. First, the CVs of blank solution (Fig. 5A. curve a) and 3.0 µM CPF solution (Fig. 5A. curve b) in 0.1 M phosphate buffer (pH 7.0) were investigated by an unmodified graphite-epoxy composite electrode in the potential range of -1.00 to -1.75 V with scan rate 50 mV s^{-1}. According to the results, CPF has an irreversible reduction peak at a potential of about -1.35 V *vs*. Ag/AgCl, which agrees with a reported paper by Karimian *et al.* [39]. This potential was used for further experiments. In addition, the MIP and HKUST-1@MIP-GECE peaks were recorded after extraction in 3.0 µM CPF solution (Fig. 5A. curve c and d). As the figure shows, the HKUST-1@MIP-GECE voltammogram shows the highest current (Fig. 5A. curve d). (Conditions of CV: the percentage of Cu-MOF@MIPs, 9%; pH of extraction solution, 6.0; pH of measuring solution, 7.0, and incubation time: 8 min). The electrochemical behavior of different prepared electrodes in the presence of CPF was also investigated by the differential pulse voltammetry (DPV) technique (Conditions of DPV: the percentage of Cu-MOF@MIPs, 9%; pH of extraction solution, 6.0; pH of measuring solution, 7.0, and incubation time: 8 min). For this purpose, the electrodes were immersed in a 25.0 µM solution of CPF prepared in 0.1 M phosphate buffer (pH 7.0). Then the DPV signal of CPF was recorded in the potential range of -1.0 to -1.7 V. A small signal is observed with unmodified GECE (Fig. 5B, curve a), where a significant signal is obtained with MIP-modified electrodes (Fig. 5B, curve b). Besides, because of the large surface area, HKUST-1@MIP-GECE (Fig. 5B, curve c) shows the most extensive cathodic current compared to the others.

Investigating the EEffect of Potential Scan Rates

Figure 6 shows the effect of potential scan rates on CPF reduction currents. As the figure shows, increasing the scan rate increases the peak reduction current of CPF. Also, there is a linear relationship between the peak current and the root of the potential scan rate ($v^{1/2}$), which indicates that the reduction of CPF is controlled by diffusion.

Optimization of Experimental Conditions

In order to obtain the highest analytical signal, the influential factors, including HKUST-1@MIP amounts, pH of rebinding solution, pH of measuring solution, and incubation time, were optimized by comparing the DPV responses of the HKUST-1@MIP graphite epoxy electrode. Different HKUST-1@MIP content (5, 6, 8, 9, 10, and 11% in graphite powder) were tested. As shown in (Fig. S4, A), the current response increases notably with HKUST-1@MIP up to 9%. It was expected because more active sites were available at the electrode surface with more HKUST-1@MIP. No additional signal was obtained with larger amounts of HKUST-1@MIP, maybe due to enough active sites in the electrode composition. However, 9% of HKUST-1@MIP was selected for further experiments. In order to optimize the pH of the rebinding solution, various experiments were done using several rebinding solutions in the pH range of 4.0 to 10.0. As shown in Fig. S4B, when the pH is increased from 4.0 to 6.0, the peak current increases and then decreases with increasing solution pH. Therefore, the optimal pH of the rebinding solution was considered equal to 6.0. Another vital factor in electrochemical measurements is the pH of the analysis solution [40,41]. Analysis was also performed at 4.0 to 10.0 to find the best pH for electrochemical measurements. According to Fig. S4C, the maximum analytical signal is achieved with a solution pH = 7.0. So, this pH value was selected for further tests. Figure S4D shows several incubation times ranging from 3 to 19 min. With increasing the incubation times up to 8 min, the peak current increases and remains constant. Therefore, 8 min was selected as the optimal incubation time.

Computational Calculations for the pH of Rebinding Solution

The pH of the medium can affect the CPF-MAA complex's stability. The stability was investigated through the number of hydrogen bonding between CPF and MAA. With the aid of the Gaussian 09 suite of programs, complexes with two hydrogen bonds were investigated (Figs. S5, S6, and S7), and related complexation energies were calculated using the equation

$$\Delta E = E_{complex} - \Sigma E_{mon}$$

$E_{complex}$ and E_{mon} are optimized energies of the CPF–MAA complex and each MAA monomer, respectively. The results in Table S1 indicate the trend in the stability of complexes in neutral, alkaline, and acidic conditions. In neutral conditions, the stability order was CPF–MAA(V) > CPF–MAA(III) > CPF–MAA(VIII) > CPF–MAA(IV) ≈ CPF–MAA(VII) >

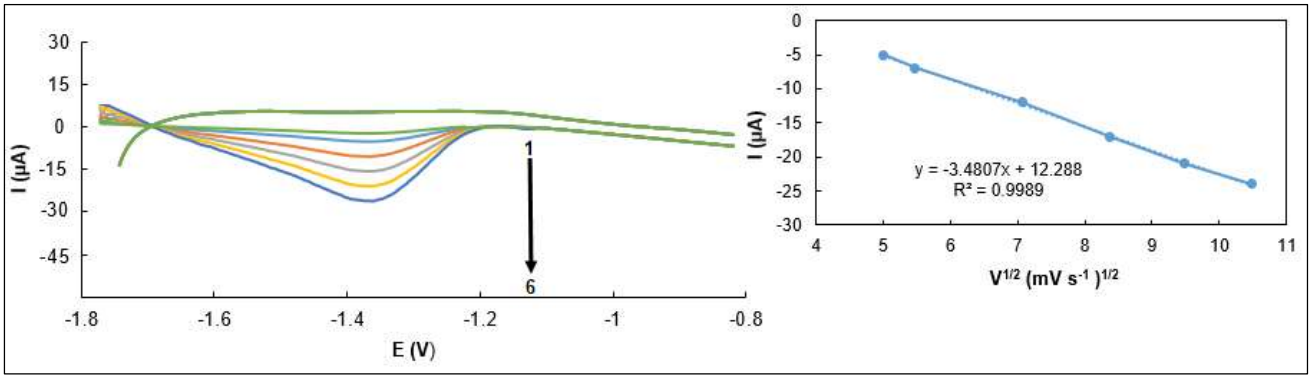

Fig. 6. CVs of Cu-MOF@MIP-GECE after extraction in 3.0 µM CPF in 0.1 M phosphate buffer (pH 7.0) containing 1 M KCl at different scan rates; numbers 1-6 according to 10, 30, 50, 70, 90, and 110. mV s^{-1}. Inset: change of cathodic peak current *vs.* $v^{1/2}$.

CPF–MAA(VI) > CPF–MAA(IX) > CPF–MAA(I) CPF–MAA(II). In alkaline conditions the trend was CPF^{-}–MAA(IV) > CPF^{-}–MAA(II) > CPF^{-}–MAA(VII) > CPF^{-}–MAA(III) > CPF^{-}–MAA(VIII) > CPF^{-}–MAA(VI) > CPF^{-}–MAA(V) > CPF^{-}–MAA(I), and in acidic conditions it was CPF^{+}–MAA(VIII) > CPF^{+}–MAA(IX) > CPF^{+}–MAA(V) > CPF^{+}–MAA(VI) > CPF^{+}–MAA(IV) > CPF^{+}–MAA(III) > CPF^{++}–MAA(VII) > CPF^{+}–MAA(II) > CPF^{+}–MAA(I). As it is shown, CPF–MAA(V), CPF^{-}–MAA(IV), and CPF^{+}–MAA(VIII) complexes are the most stable complexes in neutral, alkaline, and acidic media, respectively. A comparison between the ΔE values of these complexes indicates that the greatest tendency of molecules to interact together is obtained in acidic media. This observation is in agreement with the experimental results.

Analytical Performance of the HKUST-1@MIP Sensor

The analytical parameters were obtained under optimal conditions. The test conditions include 9% MOF for making electrodes, the pH of the extraction solution being 6, the pH of the measurement solution being 7, and the incubation time of the template molecule being 8 min, whose graphs are mentioned in the supplementary file. As shown in Fig. 7, the reduction currents have an excellent linear relationship with CPF in the concentration range of 0.05 to 40.00 µM, with a slope of -1.033 µA μM^{-1} and a correlation coefficient of 0.9983. The limit of detection (LOD) based on a signal-to-noise of 3 was estimated to be 3.0 nM. The RSD% for five successive determinations of 0.6 µM CPF was 5.37%.

The selectivity of the HKUST-1@MIP-GECE sensor was evaluated with interfering species that have a similar structure to CPF. For this purpose, the solution of 0.4 µM CPF and various concentrations of interfering species of FT, MP, PLN, and PX were analyzed. The tolerance limit was defined as the maximum interference concentration that provides less than ±5% relative error. As Table 1 shows, the presence of interfering species has no effect on the measurement of CPF at the given concentration. The result demonstrated that the proposed sensor is highly selective for measuring CPF.

Furthermore, an as-prepared sensor was used to measure 0.4 µM CPF signal each week to evaluate the stability of the fabricated electrodes. After two months the measured current responses maintain 93.2 (±3.1)% of their initial value. The result indicates that the proposed electrode is highly stable.

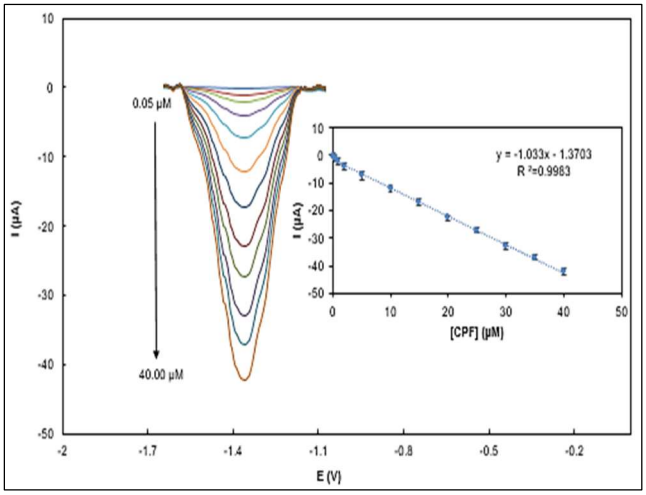

Fig. 7. DPV curves of the HKUST-1@MIP-GECE in 0.1 M PBS (pH 7.0) after rebinding different concentrations CPF in the range 0.05-40.00 µM. The inset is the calibration curve for CPF (The accumulation time of CPF is 8 min).

Table 1. Effect of Diverse Interfering Species on CPF (0.4 µM) Determination

Pesticide	Tolerance concentration (µM)	CPF signal
Fenthion	40	-2.259
Methyl parathion	50	-2.259
Phosalone	35	-2.259
Phoxim	60	-2.259

Real Sample Analysis

The preparation of apple and tomato samples was according to the real sample preparation section. After the preparation of real samples, the amount of CPF in apple and tomato samples was measured according to the optimal conditions (the percentage of Cu-MOF@MIPs, 9%; pH of extraction solution, 6.0; pH of measuring solution, 7.0, and

Table 2. Determination of CPF in Real Samples

Sample	Spiked (μM)	Found (μM)	Recovery (%)
Apple	0	-	-
	3.52	3.71	105.3
	7.4	7.5	101.3
	11.4	11.71	102.63
Tomato	0	-	-
	12.9	13.4	103.8
	17.3	17.1	98.8
	24.2	24.4	100.8

incubation time: 8.0 min) and the recovery percentages were obtained. CPF was determined in apple and tomato samples based on the proposed procedure to evaluate the practical applications. The real samples were also spiked with different amounts of CPF. As shown in Table 2, the recovery values are obtained in the range of 98.8 to 105.3%, indicating the high accuracy and reliability of the proposed electrode.

Comparison with other Analytical Methods

The performance of the proposed method for determining CPF was compared with some of the published electrochemical methods (Table 3). It can be seen that the HKUST-1@MIP-GEC electrode has the lowest LOD of the given literature studies.

CONCLUSION

This study prepared an electrochemical sensor based on a graphite-epoxy composite modified with an HKUST-1@MIP to measure CPF. The MIP coated on the surface of HKUST-1 was characterized by FESEM, FT-IR, XRD, and EDAX. HKUST-1@MIP-GEC electrode was cost-effective, and its construction using epoxy resin was easy and controllable. With ample surface area of HKUST-1 and specific binding cavities designed in MIP structure, a sensitive and selective electrode with excellent detection limit, wide dynamic range, and reasonable stability was proposed. The developed electrode can be a good candidate for analytical purposes. The HKUST-1@MIP-GECE sensor was successfully applied to analyze CPF in fruit samples.

Table 3. Comparison of the Efficiency of some Electrochemical Methods Used in the Detection of CPF

Method	Modifier	LOD	LDR	Ref.
DPV	Nano-TiO_2/ Cellulose acetate composite	3.5 μM	20.0-110 μM	[38]
CV	CO_3O_4/ PAn[a]	0.03 μM	0-28.5 μM	[42]
CV and DPV	MIP	0.004 μM	0.0001-10.0 μM	[41]
DPV	m-AgSAE[b]	2.6 μM	20-100 μM	[43]
DPV	AChE/[BMIM][BF4]- MWCNT/CPE[c]	0.004 μM	0.01-1.0 μM	[44]
EIS	PPy/PGE[d]	0.01 μM	0.06-0.9 μM	[1]
DPAdSV[e]	RGO[f]	0.2 μM	0.519-8.12 μM	[45]
			8.12-2180 μM	
DPV	HKUST-1@MIP	3.0 nM	0.05-40.00 μM	This work

[a]Cobalt oxide/Polyaniline magnetic nanoparticle, [b]Mercury meniscus modified silver solid amalgam electrode, [c]Acetylcholinesterase/1-butyl-3-methylimidazolium tetrafluoroborate/multiwalled carbon nanotube/carbon paste electrode, [d]Molecularly imprinted polypyrrole modified pencil graphite electrode,[e]Differential pulse adsorptive stripping voltammetry, [f]Reduced graphene oxide.

REFERENCES

[1] Z.O. Uygun, Y. Dilgin, Sensor. Actuat. B-Chem. 188 (2013) 78.

[2] T.C. Sparks, A.J. Crossthwaite, R. Nauen, S. Banba, D. Cordova, F. Earley, F.J. Wessels, Pestic. Biochem. Physiol. 167 (2020) 104587.

[3] W. Huang, X. Zhou, Y. Luan, Y. Cao, N. Wang, Y. Lu, W. Xu, Sep. Sci. 43 (2020) 954.

[4] M. Rahimi Moghadam, B. Zargar, S. Rastegarzadeh, Analyst 143 (2018) 2174.

[5] A.N. Adum, G. Gibson, L.M. Chimbevo, P.S. Oshule, S. Essuman, M.N. Asamba, Science 9 (2021) 88.

[6] A. Tabibi, M.T. Jafari, Food. Chem. 373 (2022) 131527.

[7] B.Y.P. Tay, W.H. Wai, Am. Oil. Chem. Soc. 98 (2021) 881.

[8] L. Nana, L. Ruiyi, W. Qinsheng, Y. Yongqiang, S. Xiulan, W. Guangli, L. Zaijun, Hazard. Mater. 415 (2021) 125752.

[9] Z. Mehrani, H. Ebrahimzadeh, A.R. Aliakbar, A.A. Asgharinezhad, Microchim. Acta 185 (2018) 1.

[10] S. Uniyal, R.K. Sharma, Biosens. Bioelectron. 116 (2018) 37.

[11] H. Saedi, M.R. Fat'hi, B. Zargar, Chin. Chem. Soc. 68 (2021) 1954.

[12] S. Zeinali, H. Khoshsafar, M. Rezaei, H. Bagheri, Anal. Bioanal. Chem. Res. 5 (2018) 195.

[13] R. Zarrin, R.E. Emamali Sabzi, Anal. Bioanal. Chem. Res. 9 (2022) 113.

[14] Z. Mirzaei Karazan, M. Roushani, Anal. Bioanal. Chem. Res. 10 (2023) 269.

[15] G. Selvolini, G. Marrazza, Sensors 17 (2017) 718.

[16] S. Bakhtiar, S.A. Bhawani, S.R. Shafqat, Chem. Bio. Tech. Agr. 6 (2019) 1.

[17] I. Bakas, A. Hayat, S. Piletsky, E. Piletska, M.M. Chehimi, T. Noguer, R. Rouillon, Talanta 130 (2014) 294.

[18] A. Poma, A. Guerreiro, S. Caygill, E. Moczko, S. Piletsky, RSC. Adv. 4 (2014) 4203.

[19] K.C. Francisco, A. Lobato, N. Tasić, A.A. Cardoso, L. M. Gonçalves, Talanta 250 (2022) 123723.

[20] M. Ahmadi, A. Mokhtari, G. Bahlakeh, H. Karimian, Luminescence 37 (2022) 1514.

[21] A.N. Hasanah, D. Soni, R. Pratiwi, D. Rahayu, S. Megantara, Chemistry 2020 (2020) 1.

[22] S. Yuan, L. Feng, K. Wang, J. Pang, M. Bosch, C. Lollar, Y. Sun, J. Qin, X. Yang, P. Zhang, Q. Wang, Adv. Mat. 30 (2018) 1704303.

[23] B. Li, H.M. Wen, Y. Yu, Y. Cui, W. Zhou, B. Chen, G. Qian, Mater. Today. Nano. 2 (2018) 21.

[24] D. Zhao, K. Yu, X. Han, Y. He, B. Chen, Chem. Commun. 58 (2022) 747.

[25] X. Ma, F. Liu, Y. Helian, C. Li, Z. Wu, H. Li, H. Chu, Y. Wang, W. Lu, M. Guo, Energ. Convers. Manage. 229 (2021) 113760.

[26] M. Gupta, Z. Zhu, D. Kottilil, B.B. Rath, W. Tian, Z.K. Tan, X. Liu, Q.H. Xu, W. Ji, J. J. Vittal, ACS. Applied. Materials & Interfaces 13 (2021) 60163.

[27] M.R. Saeb, N. Rabiee, M. Mozafari, E. Mostafavi, Mater. 14 (2021) 3652.

[28] A. Motaharian, F. Motaharian, K. Abnous, M.R.M. Hosseini, M. Hassanzadeh-Khayyat, Anal. Bioanal. Chem 408 (2022) 6769.

[29] X. Liu, L. Chen, Y. Gao, J. Li, J. Sun, T. Gan, Environ. Chem. Eng. 10 (2022) 107661.

[30] F.L. Jin, X. Li, S.J. Park, Ind. Eng. Chem. 29 (2015) 1.

[31] D. Balgude, A. Sabnis, S.K. Ghosh, Prog. Org. Coat. 104 (2017) 250.

[32] J.A. Cruz-Navarro, F. Hernandez-Garcia, G.A.A. Romero, Coord. Chem. Rev. 412 (2020) 213263.

[33] J. Tomasi, M. Persico, Chem. Rev. 94 (1994) 2027.

[34] D.M. Dolney, G.D. Hawkins, P. Winget, D.A. Liotard, C.J. Cramer, D.G. Truhlar, Comput. Chem. 21 (2000) 340.

[35] A.R. Abbasi, K. Akhbari, A. Morsali, Ultrason. Sonochem. 19 (2012) 846.

[36] A. Asfaram, M. Ghaedi, K. Dashtian, Ultrason. Sonochem. 34 (2017) 640.

[37] D. Garg, H. Rekhi, H. Kaur, K.J. Singh, A.K. Malik, Fluorescence 32 (2022) 1171.

[38] A. Kumaravel, M. Chandrasekaran, Agr. Food. Chem. 63 (2015) 6150.

[39] N. Karimian, H. Fakhri, S. Amidi, A. Hajian, F. Arduini, H. Bagheri, New J. Chem. 43 (2019) 2600.

[40] J.K. Ma, X.C. Huang, S.L. Wei, Sep. Sci. 41(2018) 3152.

[41] W. Xu, Q. Wang, W. Huang, W. Yang, Sep. Sci. 40

(2017) 4839.
[42] W.H. Wang, Z.J. Han, P.J. Liang, D.Q. Guo, Y.J. Xiang, M.X. Tian, Z.L. Song, H.R. Zhao, Nanomat. Biostruct (DJNB). 12 (2017) 1.
[43] J. Fischer, A. Hájková, M. Pereira, M. Křeček, V. Vyskočil, J. Barek, Electrochim. Acta 216 (2016) 510.
[44] L.G. Zamfir, L. Rotariu, C. Bala, Biosens. Bioelectron. 26 (2011) 3692.
[45] B. Koçak, H. Çelikkan, Int. J. Pure. Appl. Sci. 7 (2021) 1.